SCIENTIFIC REPORTS

OPEN

SUBJECT AREAS:
APPLIED PHYSICS
BIOLOGICAL SCIENCES
NETWORKS AND SYSTEMS BIOLOGY
STATISTICAL PHYSICS, THERMODYNAMICS AND NONLINEAR DYNAMICS

Received
24 March 2011

Accepted
25 July 2011

Published
12 August 2011

Correspondence and requests for materials should be addressed to Y.M. (yamir.moreno@gmail.com)

Modeling human mobility responses to the large-scale spreading of infectious diseases

Sandro Meloni[1,2], Nicola Perra[3,4], Alex Arenas[5,2], Sergio Gómez[5], Yamir Moreno[2,6] & Alessandro Vespignani[3,7]

[1]Department of Informatics and Automation, University of Rome ''Roma Tre'', Via della Vasca Navale, 79 Rome 00146, Italy, [2]Institute for Biocomputation and Physics of Complex Systems (BIFI), University of Zaragoza, 50018 Zaragoza, Spain, [3]Center for Complex Networks and Systems Research, School of Informatics and Computing & Pervasive Technology Institute, Indiana University, Bloomington, IN, USA, [4]Linkalab, Center for the Study of Complex Networks, Cagliari 09129, Sardegna, Italy, [5]Department d'Enginyeria Informàtica i Matemàtiques, Universitat Rovira i Virgili, 43007 Tarragona, Spain, [6]Department of Theoretical Physics, University of Zaragoza, 50009 Zaragoza, Spain, [7]Computational Epidemiology Laboratory, Institute for Scientific Interchange, Turin, Italy.

Current modeling of infectious diseases allows for the study of realistic scenarios that include population heterogeneity, social structures, and mobility processes down to the individual level. The advances in the realism of epidemic description call for the explicit modeling of individual behavioral responses to the presence of disease within modeling frameworks. Here we formulate and analyze a metapopulation model that incorporates several scenarios of self-initiated behavioral changes into the mobility patterns of individuals. We find that prevalence-based travel limitations do not alter the epidemic invasion threshold. Strikingly, we observe in both synthetic and data-driven numerical simulations that when travelers decide to avoid locations with high levels of prevalence, this self-initiated behavioral change may enhance disease spreading. Our results point out that the real-time availability of information on the disease and the ensuing behavioral changes in the population may produce a negative impact on disease containment and mitigation.

The inclusion of mobility processes is a key ingredient in the modeling of the geographic spread of epidemics. Recently this has been made evident in the modeling effort concerned with the diffusion of the 2009 H1N1 pandemic in which several papers have obtained estimates of the epidemic parameters and unfolding based on the knowledge of human travel and mobility patterns[1–3]. Models that explicitly take into account the mobility patterns of individuals range from relatively coarse-grained approaches that consider aggregated traveling flows to highly detailed structured metapopulation or agent-based models allowing for the description of billions of individuals[4–6]. However, the available data on human mobility and interaction are descriptive of human behavior as long as information concerning the unfolding of the epidemic does not induce changes in the population's behavior, for at this point the model has to include the population's behavioral changes that in turn alter the epidemic spreading. Although behavioral changes are in many cases triggered by the policy-making effort of public institutions and agencies, self-initiated changes in behavior induced by transmission of information about the disease both from the media and the local environment (friends, colleagues, etc.) are often initiated by the population's individuals. Self-initiated behavioral changes are elusive to modeling because of the difficulty involved in quantifying these changes and an overall lack of relevant data. In this case mathematical and computational modeling represents a very effective tool for exploring the impact of behavioral changes on the epidemic. For this reason there has been an increasing focus in the development of formal models aimed at closing the epidemic-spreading→behavioral-changes→epidemic-spreading feed-back loop for the past decade (see[7] for a recent review). However, only a few of these theoretical and computational approaches have considered the spatially structured nature of populations and the effect of behavioral and mobility changes in the large-scale spreading of the epidemic[8–10].

Here we consider a metapopulation model that incorporates self-initiated changes in human behavior in response to an epidemic outbreak and study how these reactions influence the spread of infectious diseases. The model is general enough to include a number of different behavioral responses. Ultimately, we find that

prevalence-based behavioral changes do not affect the invasion threshold, although the number of subpopulations affected by the outbreak does depend considerably on population behavior. In particular, we introduce a simple mechanism that provides individuals with the propensity to avoid locations affected by the epidemic. Although the aim of such a self-initiated behavior is to prevent an invididual's exposure to the disease, it may lead to the unanticipated effect of facilitating its spread to new locations. The results presented in this paper underline the importance of the proper consideration of self-initiated behavioral responses to the spreading of epidemics.

Results

In order to describe the large-scale spreading of infectious diseases mathematically we use a metapopulation approach[11]. This framework describes a set of spatially structured interacting subpopulations as a network whose links denote the mobility of individuals across subpopulations. Each subpopulation consists of a number of individuals that are divided into several classes according to their dynamical state with respect to the modeled disease – for instance: susceptible, infected, removed, etc. The internal compartmental dynamics models the contagion dynamics by considering that people in the same subpopulation are in contact and may change their state according to their interactions and the disease dynamics. Finally, subpopulations also interact and exchange individuals due to mobility from one subpopulation to another. Figure 1 shows a schematic representation of the metapopulation system. The global invasion threshold that marks the point beyond which a local outbreak reaches other subpopulations and spreads throughout the metapopulation system not only depends on the infection parameters, but on the mobility rates of individuals as well[12,13] and thus differs from the single population epidemic threshold. Previous works have considered fully Markovian dynamics for the movement of individuals among subpopulations, and more recent analyses have focused on the analytical description of models with recurrent patterns.

The model and the invasion threshold. Here we consider a general scenario in which individuals have memory of their original subpopulations, which they return to after having reached their destination location. More explicitly, we define a population of size N partitioned into V subpopulations. An individual is assigned its origin destination – its *home* – among the V subpopulations. The subpopulations are interconnected by edges that represent the mobility connections among subpopulations. We can therefore see the metapopulation system as a network made of V nodes and an assigned degree distribution $P(k)$ that defines the probability that any given subpopulation is connected to k other subpopulations. Given the set of populations we can denote the number of subpopulations with k connections by V_k. A standard convenient representation of such a system is provided by quantities defined in terms of the degree k:

$$N_k = \frac{1}{V_k} \sum_{i|k_i=k} N_i \qquad (1)$$

The quantity N_k indicates the average number of individuals in a population of degree k. This is a mean-field approximation that considers all subpopulations with a given degree k as statistically equivalent, thus allowing for the introduction of degree-block variables that depend only upon the subpopulation degree. While this is an obvious approximation to the system description, it has been successfully applied to many dynamical processes on complex networks and it is rooted in the empirical evidence presented in the analysis of mobility networks[14–18]. In the following we assume the population distribution

$$N_k = \overline{N} \frac{k}{\langle k \rangle}, \qquad (2)$$

where $\overline{N} = \sum_k N_k P(k)$ is the average number of individuals per node in the subpopulation network. The mobility of the population is defined as follows: for every time step each of the N_i individuals ($N = \Sigma_i N_i$) of subpopulation i travels with probability $\lambda_{ij} = \lambda$. For

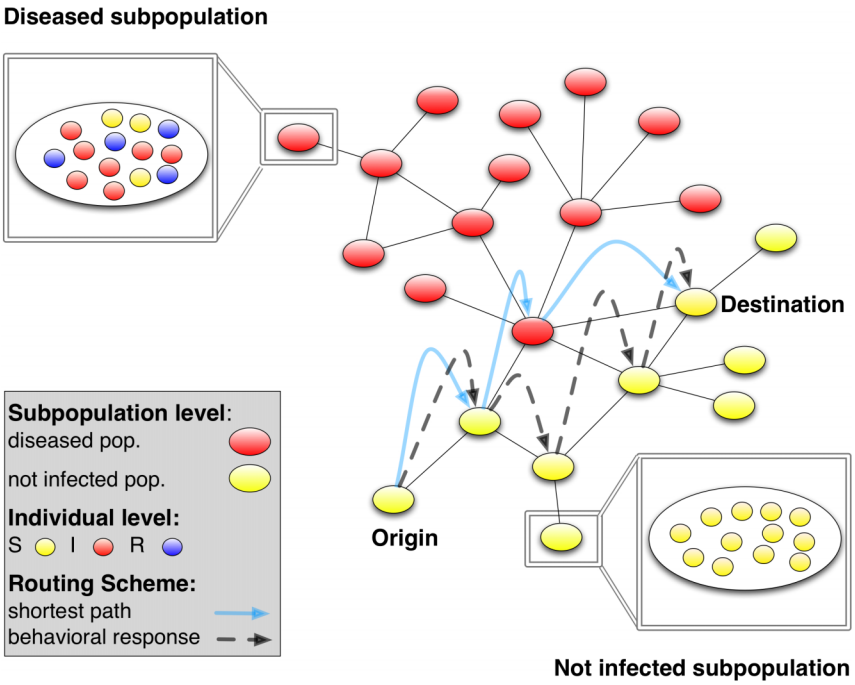

Figure 1 | Schematic representation of the Metapopulation System. A population of individuals is divided into V subpopulations connected with each other following a heterogeneous network. Within each subpopulation, individuals are classified according to their dynamical status as Susceptible (S), Infected (I) and Removed (R). In absence of behavioral changes (blue arrows), individuals move from a subpopulation to another at a rate λ following the shortest path connecting both subpopulations. The discontinuous arrows represent the second mechanism of behavioral reaction in which people travel avoiding places with high prevalence at the cost of larger diffusion paths.

simplicity, let us first consider the case in which destinations j are randomly chosen proportionally to the size of the population of the destination node (similar results are obtained by choosing the destination randomly). Individuals then move along the shortest paths to their destination nodes. This is a plausible assumption that corresponds to a traffic of individuals on each edge proportional to the edge betweenness. Data on the real network confirm this assumption with a linear statistical association between traffic flows and betweenness in the airport network (see supplementary online information). Additionally, once a traveler arrives at its destination, it must return to its origin subpopulation along the same shortest route.

For the epidemic dynamics in each subpopulation i we first consider the minimal SIR (Susceptible Infected Removed) model, according to which individuals are partitioned into $S_i(t)$, $I_i(t)$, and $R_i(t)$ compartments, denoting the number of susceptible, infected, and removed individuals at time t, respectively. The transition rate from the susceptible to the infected state is given through the usual force of infection $\beta I_i/N_i$, while infected individuals recover at a rate μ. The SIR model[11,19] is characterized by the average number of infectious individuals produced by a single infected individual in a fully-susceptible population, the so-called reproductive number $R_0 = \beta/\mu$. In a stochastic model if $R_0 > 1$ an outbreak may take place[11,19]. For the case of metapopulation models, the previous condition on R_0 for the subpopulation outbreak holds. However, if the mobility rate of the individuals of the originally infected subpopulation is not enough to ensure the seeding of other subpopulations before the waning of the local epidemic, the outbreak does not spread globally. This is equivalent to the existence of a second reproductive number at the subpopulation level R^* that depends on the mobility parameters and defines the threshold for the epidemic invasion of a finite fraction of subpopulations[12,20–22].

In order to derive the condition for global spread in our model with origin-destination dynamics let us consider a metapopulation system in which a small set of initially infected subpopulations $\{D_k^0\}$ is experiencing an outbreak with $R_0 > 1$. In the early stage of the epidemic, the number of subpopulations experiencing an outbreak is small and we describe the disease spreading at the level of the metapopulation system as a branching process, using a tree-like approximation relating the infected subpopulations D_k^n at generation n to the infected subpopulations D_k^{n-1} at generation $n-1$. The average number of infected individuals in subpopulations of degree k during the evolution of the epidemic is αN_k, where α is a disease-dependent parameter expressing the total number of individuals in the population that have been in the infectious state. Furthermore, in the SIR model, each infected individual stays in the infectious state for an average time μ^{-1}. Thus, the total number of infected individuals circulating through the network at the $n-1$ generation is:

$$\omega^{n-1} = \frac{\lambda\alpha}{\mu}\sum_{k'} D_{k'}^{n-1} N_{k'} \tag{3}$$

Those individuals can trigger the start of an epidemic in a non-infected subpopulation with probability $[1-R_0^{-\gamma}]$, where γ is the number of infectious individuals in generation $n-1$ that have visited the subpopulation[23]. In order to provide a quantitative estimate of this number we consider that if individuals follow the shortest route through the network, then the probability that a node of degree k is visited by any individual is proportional to the average betweenness b_k of nodes of corresponding degree. This allows us to write explicitly (as shown in the material and methods section) the branching ratio that provides the average number of subpopulations that will be infected by each subpopulation experiencing an outbreak, defining the following global invasion threshold:

$$R^* = (R_0 - 1)\frac{\lambda\alpha}{\mu}\bar{N}\frac{1}{\langle k\rangle}\frac{\langle k^{1+\eta}\rangle}{\langle k^{\eta}\rangle} \geq 1, \tag{4}$$

which can also be expressed as a threshold condition for the mobility rate λ as

$$\lambda\bar{N} \geq \frac{\langle k^{\eta}\rangle}{\langle k^{1+\eta}\rangle}\frac{\langle k\rangle\mu}{\alpha}(R_0-1)^{-1}. \tag{5}$$

This threshold condition is extremely relevant as it links the mobility rate and patterns of individuals to the eventual global spreading of the disease. This allows us to relate the mobility of individuals to the global spreading of the disease and eventually study how behavioral changes that affect human mobility may alter the course of epidemic outbreaks. As we have previously detailed, the analytic calculations are based on several simplifications and assumptions and reduce to the critical point of a simple branching process. In order to test the robustness and reliability of the calculation we compare results from individual-based simulations in Fig. 2 with the analytic prediction expressed in Eq.(5). The individual-based simulations are detailed in the Materials and Methods section and are based on stochastic and discrete binomial models of transmission and mobility[24,25]. Here we report networks of size $V = 3{,}500$ with $N = 3\times10^6$ individuals. These relatively small sizes are the most interesting as the mean-field approximations used in the calculations are obviously valid in the case of large-scale random graphs. The figure shows that the mean-field framework nicely estimates the value of the mobility threshold beyond which the movement of individuals from infected subpopulations to susceptible ones is large enough as to seed the latter and spread the epidemic to a system-wide scale. For the sake of completeness we report simulations in the supplementary online material for sizes up to $V = 3\times10^4$ and $N = 3\times10^7$ that confirm the analytical results.

Self-initiated behavioral changes. During the outbreak of an acute infectious disease it is natural to expect self-initiated human behavioral changes and variations of individuals' mobility patterns. Obviously the extent of behavioral change depends on the risk as perceived by individuals that concerns the severity of the disease, prevalence of it within the population, and the information available on the disease. Behavioral changes have been shown[7] to modify the disease state of individuals[26,27], model parameters[28] and contact structure[29]. In our system human responses to the presence of a disease might have a direct impact on mobility and traveling habits, since avoiding infected areas is a natural attitude of individuals and more drastic reactions such as not traveling at all may spontaneously arise, as documented in the recent epidemic. In

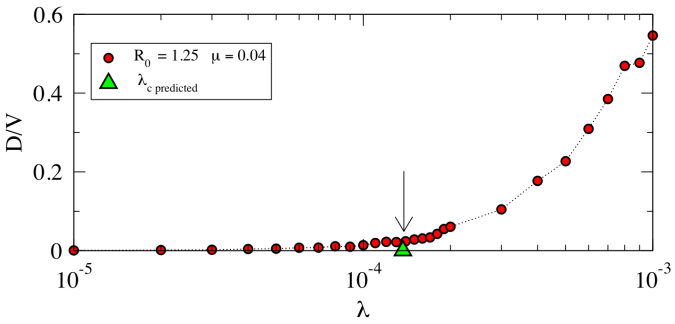

Figure 2 | Mobility Threshold. To compare the analytical insights with numerical results here we represent the number of diseased subpopulations D/V as a function of the mobility rate λ. The analytical value (Eq.(5)) is indicated by the arrow and the green triangle. Full circles are results from numerical simulations and represent the average over at least 100 stochastic runs (the line is a visual guide). The value of α has been approximated by $\alpha = 2(R_0-1)/R_0^2$ [19]. The substrate topology is an uncorrelated scale-free network generated according to the uncorrelated configuration model[30] with $\gamma = 2.5$, $V = 3000$ subpopulations and $N = 3\times10^6$ individuals. Other parameters are indicated in the figure.

order to model behavioral changes in our framework we consider that individuals react to prevalence-based information and study two mechanisms of behavioral change. The simplest one assumes that the probability $p_{ij}(t)$ of traveling from subpopulation i to subpopulation j at time t is related to the level of infection at the destination subpopulation so that the higher the incidence of the infection at the destination, the less likely the individual will engage in traveling, i.e., $p_{ij}(t) = 1 - I_j(t)/N_j(t)$. If travel is not cancelled, then the individual moves following the shortest path to the destination. This mechanism is the one that has led to the decline in the number of passengers arriving at airports in Mexico both domestically and internationally in 2009 due to the H1N1 influenza outbreak.

The second mechanism of mobility change (see Fig. 1) models behavioral reactions that induce changes in traveling routes. Specifically, given an individual who is traveling from an origin (subpopulation i) to a destination (subpopulation j), we assume that it will try to avoid traversing infected nodes, except when the next move leads to its destination. This process is obviously not deterministic and it consists of a trade-off between the risk associated with visiting a given subpopulation and the increase of the travel path length to the final destination. We assume that the risk perception associated with the visit of a given subpopulation is dependent on the prevalence of the disease in that subpopulation. However, staying away from infected subpopulations has the associated cost of traveling through alternative routes. We therefore assume that individuals move to the neighboring subpopulation l that minimizes the cost function $c_l(t) = h\delta_l + (1-h)I_l(t)/N_l(t)$, where δ_l is the change in distance to the destination, which can only take values -1 if node l is in the shortest path to the destination, 0 if it is at the same distance to the destination than the actual node, and +1 otherwise. The parameter h tunes the force of the behavioral response and for $h = 1$ the shortest path is always followed, whereas $h = 0$ corresponds to a path minimizing the risk of traversing infected areas.

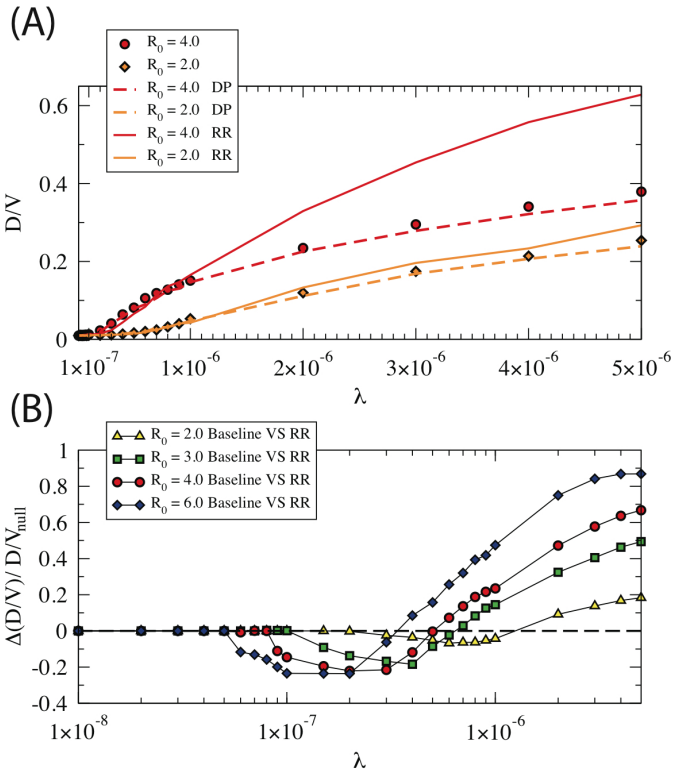

Figure 3 | Effects of behavioral changes in synthetic networks. The figure compares the fraction of diseased subpopulations D/V when behavioral reaction mechanisms are active with the situation in which such behavioral responses are not taken into account (null model). (A) We show the dependency of D/V with the mobility rate λ (A) for random scale-free networks generated according to the uncorrelated configuration model[30]. Symbols represent the results obtained when individuals do not react to the presence of the disease (error bars are smaller than symbol sizes). The rest of the results correspond to the mechanisms of behavioral changes: "DP" stands for "departure probability" and represents the mechanism in which individuals decide whether or not to travel; "RR" (rerouting) corresponds to the case in which people travel while trying to minimize the risk of infection avoiding subpopulations with high prevalence at the cost of long travel paths. The results confirm that the invasion threshold is independent of behavioral changes and that the latter has a significant impact on the invasion dynamics of the metapopulation. The points are the averages among at least 100 stochastic runs and we consider $\mu = 0.04$ and $h = 0.1$. See the main text for further details. (B) we report the relative difference of subpopulations experiencing an outbreak in the RR and baseline scenarios as a function of λ. It is possible to see the non-linear behavior that first induces a decrease – close to the invasion threshold – and then a sharp increase in the number of affected subpopulations.

Synthetic metapopulation system. As for the analysis of the global invasion threshold, we simulate a metapopulation network of $V = 3000$ nodes and $N = 3\times10^6$ individuals as detailed in the Materials and Methods section. In Figs. 3 and 4 we report the behavior of the density of infected subpopulations D/V at the end of the global epidemic as a function of both the basic reproductive number R_0 and the traveling diffusion rate λ. The curves report the baseline case without behavioral changes and the case in which behavioral changes are implemented. The results readily show that in all analyzed cases the metapopulation system exhibits an invasion threshold which is independent of human behavioral changes. This feature of the model can be traced back to the fact that the behavioral changes are prevalence based. Analogously to the basic reproductive number, the invasion threshold is determined by the average number that each infected subpopulation will generate in a fully susceptible metapopulation system. Clearly in this regime the prevalence-based behavioral changes are irrelevant and the threshold value is thus not affected. As we increase the value of the parameters above the epidemic threshold we start observing differences in the two cases with respect to the number of subpopulations affected by the epidemic. In particular, it is not difficult to separate the effects of

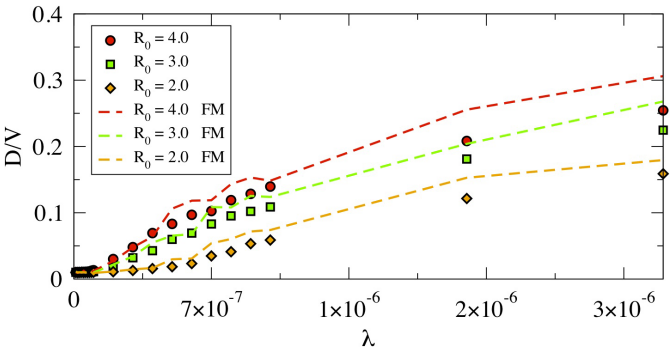

Figure 4 | Effects of behavioral changes in data-driven scenarios. Comparison of the fraction of diseased subpopulations D/V for the full (behavioral reaction mechanisms are active) and null (behavioral responses are not taken into account) limits of the metapopulation system. We plot D/V as a function of the mobility rate λ. The results confirm even in this case that the invasion threshold is independent of behavioral changes. Moreover, as for synthetic networks, epidemic awareness enhances the disease spreading as given by the increase in the number of subpopulations affected by the disease. The averages were taken over at least 100 stochastic realizations and we fix $\mu = 0.04$ and $h = 0.1$. See the main text for further details.

the two mechanisms of behavioral changes. When people have the option of deciding whether or not to engage in travel, the fraction of diseased subpopulations at the end of the outbreak decreases with respect to the null case, thus pointing out that this kind of response is beneficial. The reason for the reduction in D/V is rooted in the effective reduction of the mobility rate of individuals, which leads to a smaller exposure of susceptible individuals to the disease both while traveling and at home. A different scenario emerges in the case that individuals attempt to avoid infected subpopulations. For values of the parameter R_0 and λ close to the invasion threshold the rerouting of individuals on different paths leads to a reduction of the outbreak probability $(1-R_0^{-\gamma})$ in the subpopulations along the origin-destination path. This leads to a final reduction of the subpopulations experiencing an outbreak. For increasing R_0 and λ this probability saturates to one and all subpopulations visited on the original and the rerouted path experience an outbreak. In this regime the number of subpopulations affected by the epidemic is much larger than the case without behavioral changes. The enhancement of the epidemic size is visible in Fig. 3 and occurs close to the invasion threshold onward. A full discussion with analytical arguments of this behavior is provided in the supplementary online material, and points out the important and counter-intuitive effects that may be generated by behavioral changes in the population.

Data-driven simulations. While the previous set of computational studies are obtained in a synthetic and in some ways simplified metapopulation scheme, we also carried out Monte Carlo simulations using the Air Transportation Network (see Materials and Methods). This network is highly heterogeneous with respect to the number of connections between urban areas (subpopulations) as well as the traffic w_{il} in terms of the number of passengers and available seats on a given direct route connecting two subpopulations i and l. Taking into account these traffic patterns, we assume that initially the number of individuals in subpopulation i is proportional to its strength $N_i = \Sigma_l\, w_{il}$. In this realistic setting, instead of using a shortest-path routing we implement a traffic-based routing where individuals follow paths to the destination proportionally to the actual traffic to the destination. Moreover, as the travel flows are not homogeneous, we also consider that individuals choose their destinations proportionally to the strengths of each possible target subpopulation and that all travelers spend a time τ at their destinations before coming back home. In this way, we preserve the inter-city traffic patterns. The parameter τ is drawn from a uniform distribution with mean equal to the traveled distance d_{il}. Sensitivity analyses for these parameters and those defining the behavioral changes are reported in the Supplementary Information file, where we also report the simulation for a more realistic model with the additional class of exposed individuals (the SEIR model) added to disease natural history. In Fig. 4 we report the results obtained for the data-driven model where all mechanisms of behavioral changes are at work, confirming the results obtained for the synthetic metapopulation network. We observe: i) a global invasion threshold that does not depend on behavioral changes; and, ii) that changes in traveling routes dominate the model behavior by considerably enhancing the spread of epidemics affecting a number of subpopulations compared to the case with no behavioral changes.

Discussion

The results provided by the analysis of the effect of behavioral changes in both synthetic and data-driven simulations make it clear that behavioral changes inspired by the best intention of slowing down and containing the epidemic may give rise to the opposite effect. The numerical analysis shows that the disease spreading, as given by the number of subpopulations with local outbreaks, increases when travelers decide to bypass the subpopulations with a high number of infected individuals. The behavioral change effect is clearly observed in the data-driven simulations by plotting the invasion tree in the USA with an epidemic starting in New York. The invasion tree specifies the disease progression by defining a directed link $i \rightarrow j$ from the infecting to the infected subpopulation, i.e. the origin subpopulation i of the infected individuals who have started the epidemic to the subpopulation j. Fig. 5A shows that in the absence of behavioral changes the infection tree is heterogeneous and has several hubs. This is not the case in the presence of behavioral changes where the entire tree originates from the initially infected subpopulation as shown in Fig. 5B. The rationale behind this finding is that the increased flow of individuals going through alternative paths brings the infection to new subpopulations that would otherwise be infected by other subpopulations. This constitutes a very interesting finding, as one can think of the whole process in terms of a social dilemma; individuals adopt a sort of selfish behavior by avoiding highly infected spots, but as a consequence, the disease invades a larger fraction of the subpopulations in the metapopulation system. Thus, what is beneficial at the individual level, turns out to have a negative impact on the whole population, especially in the cases where the epidemic has pervaded the system (large R_0 and λ). As Figs. 3 and 4 show, it is also worth stressing that the effects of this kind of behavioral change depend nontrivially on both R_0 and λ. Moreover, the features observed here are emphasized by models that take into account a natural history of the disease that allows for exposed individuals to become infectious after a latency period. Those individuals are subject to behavioral changes that make them avoid subpopulations that are already infected, but they do not have limitations to their mobility, thus providing an even more efficient mechanism for the large-scale spreading of the infectious disease.

The present finding points out the importance and relevant effects of behavioral changes. Other behavioral reactions may be considered separately or in concomitance with the mechanisms studied here, thus providing more complicated dynamic behavior. The addition of simple behavioral models in the analysis of the geographical spreading of infectious diseases opens the path to a multitude of effects that can have a major impact in both our understanding of epidemiological data and in the definition of public health intervention.

Methods

Invasion threshold. In order to relate the global epidemic spreading with the network betweenness we note that the number of seeding infectious individuals for each node of degree k is $\gamma_k = \frac{b_k}{b_{tot}}\,\omega^{n-1}$ where b_k is the algorithmic betweenness (equal to the topological betweenness in the case of shortest path routing) of subpopulations of degree k, and b_{tot} is the normalization factor accounting for the betweenness of all nodes. For reproductive numbers close to the epidemic threshold $(R_0 \simeq 1)$ we can approximate the infection probability (see the SI file) and write explicitly the recursive expression for the number of infected subpopulations with degree k at the nth generation as

$$D_k^n \simeq V_k(R_0-1)\,\frac{b_k}{b_{tot}}\,\frac{\lambda\alpha}{\mu}\sum_{k'} D_{k'}^{n-1} N_{k'}\,. \qquad (6)$$

It is important to remark again that this expression is obtained by assuming that the network is random, nodes with a given degree k are statistically equivalent, and the number of infected subpopulations is negligible with respect to the total number of subpopulations so that $\left(1-\sum_k \frac{D_k^{n-1}}{V_k}\right) \simeq 1$. This also allows us to consider the branching process as uncorrelated and the seeding of each subpopulation as an independent event. Furthermore, in this case it is possible to use the general result $b_k \sim k^n$ relating the node betweenness and degree in random networks. The above expression yields the branching ratio used to calculate the invasion threshold.

Internal nodes' dynamics. In each node an SIR dynamics takes place over a well-mixed population of initial size N_i. As time passes, $N_i(t)$ changes according to the number of individuals that have been received and that have left the node. Within the nodes, one step of an SIR process takes place. The state of every individual inside a node i is changed according to the following probabilities: a susceptible individual becomes infected with probability $p^{(S\rightarrow I)} = 1-\left(1-\frac{\beta}{N_i}\right)^{I_i}$, and an infected individual recovers with probability $p^{(I\rightarrow R)} = \mu$. Specifically, the exact number of individuals that change state is determined by a binomial distribution with the probability $p^{(S\rightarrow I)}$ (or $p^{(I\rightarrow R)}$) and the susceptible populations size $S_i(t)$ (or infected $I_i(t)$) as parameters. Note that in this scenario, R_0 only participates in the internal dynamics; individuals

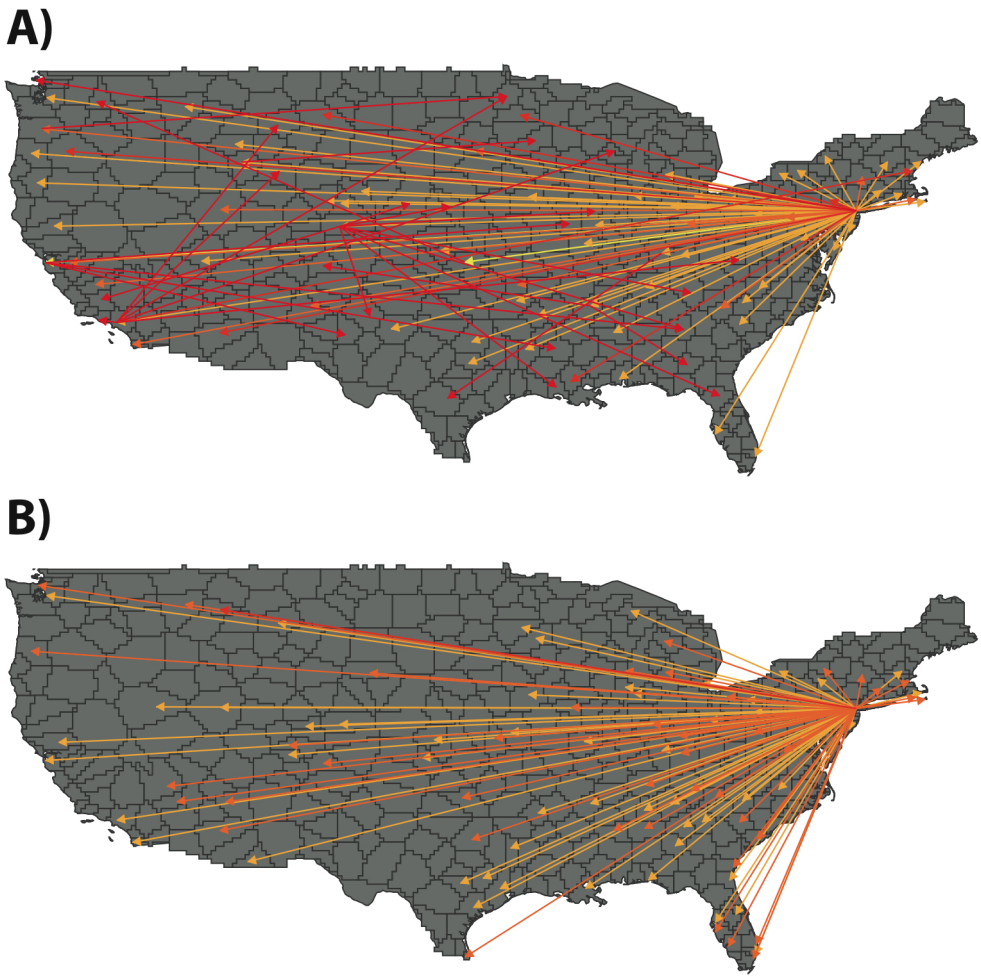

Figure 5 | Invasion tree. Invasion tree describing the air transportation network inside the USA of an epidemic starting in New York. The invasion tree specifies the disease progression by defining a directed link $i \rightarrow j$ from the infecting to the infected subpopulation. In panel (A) we show the invasion tree for the null model when no behavioral reactions are considered. In panel (B) we show the invasion tree starting from the same initial conditions but consider both mechanisms of behavioral reaction to be active. In order to provide a clear representation we consider in both cases just the first 100 infected nodes among the total 425 in a single run, respectively. The color scale is a measure of time and is the same for both cases. At the time step in which the first subpopulation is infected from the seed it is yellow. At the time step in which the last subpopulation (among the first 100 in both cases) is infected it is red. All the other time steps are in the gradient between these two limits. Panel (A) shows clearly that in the absence of behavioral changes the infection tree is heterogeneous and contains several hubs that are infected first and that determine the time scale of the spreading infection to smaller airports. This is not the case in the presence of behavioral changes where the entire tree originates and grows much faster from the initially infected subpopulation as shown in panel (B). In both cases, we fix the parameters to $R_0 = 2$, $\mu = 0.04$ and $\lambda = 10^{-6}$.

traveling through node i are involved in the SIR and thus can change their state while at node i.

Synthetic networks. We consider topologically-uncorrelated random graphs generated by an uncorrelated configuration model[30]. The simulations presented here consider a degree distribution $P(k) \sim k^{-\gamma}$ with $k_{\min} \leq k \leq k_{\max}$ and $\gamma = 2.5$ and $k_{\min} = 2$. The population of each node is assigned according to Eq. (2).

Airports network. The airport network data set is composed of passenger flights operating in the time period November 1, 2000 to October 31, 2001 as compiled by OAG Worldwide (Downers Grove, IL) and analyzed previously in Ref. 31. It consists of 3,618 nodes (airports) and 14,142 links. We use a weighted network in our analysis. Airports corresponding to a metropolitan area have been collapsed into one node in the original database.

Computational implementation. Each simulation starts with a small number of infected individuals. Specifically, we randomly choose a small fraction of subpopulations (less than 1% of the nodes) and within these subpopulations only 1% of the individuals are infected, assuring that the condition $I_0 > \frac{\mu}{\beta}$ is fulfilled. In the simulations the traffic and spreading dynamics have the same time scale, so at each time step a diffusion step is performed first and then the SIR internal dynamics is evaluated. For the diffusion of individuals we assume that the number of individuals starting a trip at time t is given by a binomial distribution with mobility rate λ and subpopulation size $N_i(t)$ as parameters. Destinations are chosen according to the strength w_i of each node. To keep the nodes' populations constant over time (excluding transient individuals traveling through the node), once an individual reaches its destination it starts a new trip back to its origin. Simulations run until the stationary state $I(t) = 0$ is reached. Note that in this framework only travelers are explicitly followed and that we only keep a counter for the number of non-traveling individuals inside each node. Individuals are labeled according to their origin population and both the disease dynamics and the mobility process are simulated with discrete, binomial processes (See Materials and Methods). Finally, simulations of the behavioral changes are made more realistic by considering that infected individuals diffuse at a lower rate, λ^I, than susceptible subjects. This simulates the fact that most of the infected individuals will exhibit symptoms that prevent them from traveling. This happens in influenza-like diseases where only a fraction of infected individuals is asymptomatic and can continue with regular mobility habits. Without loss of generality we assume that $\lambda^I = \lambda/2$ and we report in the supplementary online material the sensitivity analysis for different values of this parameter. In synthetic networks agents select which neighbor to visit next on their ways to their destinations, presuming that following the shortest path is the preferred solution in an infection-free scenario. In the simulated airport network individuals are routed proportionally to real traffic edges and individuals traveling between subpopulations are tracked in time and the evolution of the disease is monitored. In addition, we study the invasion dynamics and measure the number of diseased subpopulations at time t, $D(t)$. All numerical results reported henceforth are averages taken over at least 100 realizations of the initial conditions and the stochastic dynamics.

1. Graske, T. *et al*. Assessing the severity of the novel A/H1N1 pandemic. *BMJ* **339**, b2840 (2009).
2. Balcan, D. *et al*. Seasonal transmission potential and activity peaks of the new influenza a(h1n1): a monte carlo likelihood analysis based on human mobility. *BMC Medicine* **7**, 45 (2009).
3. Lipsitch, M., Lajous, M., O'Hagan, J. J., Cohen, T., Miller, J. C. Use of cumulative incidence of novel influenza A/H1N1 in foreign travelers to estimate lower bounds on cumulative incidence in Mexico. *PLoS ONE* **4**(9), e6895 (2009).
4. Ferguson, N. M. *et al*. Strategies for containing an emerging influenza pandemic in Southeast Asia. *Nature* **437**, 209–214 (2005).
5. Epstein, J. M. *et al*. Controlling Pandemic Flu: The Value of International Air Travel Restrictions. *PLoS ONE* **2**(5), e401 (2007).
6. Colizza, V., Barrat, A., Barthelemy, M., Valleron, A. J., Vespignani, A. Modeling the Worldwide Spread of Pandemic Influenza: Baseline Case and Containment Interventions. *PLoS Med* **4**(1), e13 (2007).
7. Funk, S., Salathé, M., Jansen, V. A. A. Modelling the influence of human behaviour on the spread of infectious diseases: a review. *J. R. Soc. Interface* **7**, 1247–1256 (2010).
8. Epstein, J. M., Parker, J., Cummings, D., Epstein, J. M., Parker, J., Cummings, D., Hammond, R. A. Coupled Contagion Dynamics of Fear and Disease Mathematical and Computational Explorations. *PLoS ONE* **3(12)**, e3955 (2008).
9. Bootsma, M. C. J., Ferguson, N. M. Public Health Interventions and Epidemic Intensity During the 1918 Influenza Pandemic. *Proc. Natl Acad. Sci. USA* **104**, 7588–7593 (2007).
10. Bajardi, P. *et al*. Human Mobility Networks, Travel Restrictions, and the Global Spread of 2009 H1N1 Pandemic. *PLoS ONE* **6(1)**, e16591 (2011).
11. Keeling, M. J., Rohani, P. *Modeling Infectious Diseases in Humans and Animals*. Princeton University Press, Princeton, 1st Edition (2007).
12. Colizza, V., Vespignani, A. Epidemic modeling in metapopulation systems with heterogeneous coupling pattern: theory and simulations. *J. Theor. Biol.* **251**, 450–467 (2008).
13. Colizza, V., & Vespignani, A. Invasion threshold in heterogeneous metapopulation networks. *Phys. Rev. Lett.* **99**, 148701 (2007).
14. LLoyd, A. L., May, R. M. How viruses spread among computers and people. *Science* **292**, 1316–1317 (2001).
15. Pastor-Satorras, R., Vespignani, A. Epidemic spreading in scale-free networks. *Phys. Rev. Lett.* **86**, 3200–3203 (2001).
16. Meloni, S., Arenas, A., Moreno, Y. Traffic-driven epidemic spreading in finite-size scale-free networks. *Proc. Nat. Acad. Sci. USA* **106**, 16897-16902 (2009).
17. Brockmann, D., Hufnagel, L., Geisel, L. The scaling laws of human travel. *Nature* **439**, 462–465 (2006).
18. Eubank, S. *et al*.Modelling disease outbreaks in realistic urban social networks. *Nature* **429**, 180–184 (2004).
19. Murray, J. D. *Mathematical Biology*, Springer-Verlag, 3rd Edition (2007).
20. Ball, F., Mollison, D., Scalia-Tomba, G. Epidemics with two levels of mixing. *Ann. Appl. Probab.* **7**, 46–89 (1997).
21. Cross, P., Lloyd-Smith, J. O., Johnson, P. L. F., Wayne, M. G. Duelling timescales of host movement and disease recovery determine invasion of disease in structured populations. *Ecol. Lett.* **8**, 587–595 (2005).
22. Cross, P., Johnson, P. L. F., Lloyd-Smith, J. O., Wayne, M. G. Utility of R_0 as a predictor of disease invasion in structured populations. *J. R. Soc. Interface* **4**, 315–324 (2007).
23. Bailey, N. T. *The mathematical theory of infectious diseases.* Hafner Press/ MacMillian Pub. Co., 2nd edition (1975)
24. Longini, I. M. Chain Binomial Models, in The Encyclopedia of Biostatistics, Volume 1, eds Armitage P., Colton T., *Wiley*, New York, 593–597 (1998).
25. Halloran, M. E., Longini, Jr. I. M., Struchiner, C. J., Binomial and Stochastic Transmission Models, in *Design and Analysis of Vaccine Studies*, eds Halloran, M. E., Longini, Jr., I. M., Struchiner, C. J. Springer, New York, 63–84 (2010).
26. Funk, S., Gilad, E., Watkins, C., Jansen, V. A. A. The spread of awareness and its impact on epidemic outbreaks. *Proc. Nat. Acad. Sci. USA* **106**, 6872–6877 (2009).
27. Eames, K. T. D. Networks of influence and infection: parental choices and childhood disease. *J. R. Soc. Interface* **6**, 811–814 (2009).
28. Coelho, F. C. & Codeo, C. T. Dynamic modeling of vaccinating behavior as a function of individual beliefs. *PLoS Comput. Biol.* **5(7)**, e1000425 (2009).
29. Gross, T., D'Lima, C. J. D. & Blasius, B. Epidemic dynamics on an adaptive network. *Phys. Rev. Lett.* **96**. 208701 (2006).
30. Catanzaro, M., Boguña, M., Pastor-Satorras, R. Generation of uncorrelated random scale-free networks. *Phys. Rev. E* **71**, 027103 (2005).
31. Guimerà, R., Mossa, S., Turtschi, A. & Amaral, L. A. N. The worldwide air transportation network: Anomalous centrality, community structure, and cities' global roles. *Proc. Natl. Acad. Sci. USA* **102**, 7794–7799 (2005).

Acknowledgements

S. G and A. A. are partially funded by FIS2009-13730-C02-02 and the Generalitat de Catalunya 2009-SGR-838. Y. M. is supported by the Spanish MICINN through projects FIS2008-01240 and FIS2009-13364-C02-01 and by the Government of Aragón (DGA) through the grant No. PI038/08. A.V. is partially funded by the NIH R21-DA024259 award and the DTRA-1-0910039 award. The work has been also partly sponsored by the Army Research Laboratory and was accomplished under Cooperative Agreement Number W911NF-09-2-0053. The views and conclusions contained in this document are those of the authors and should not be interpreted as representing the official policies, either expressed or implied, of the Army Research Laboratory or the U.S. Government.

Author Contributions

A.A, S.G, Y.M & A.V designed research, S. M & N.P performed research, S.M, N.P, A.A, S.G, Y.M & A.V analyzed the data, S. M, N.P, Y.M & A.V contributed new analytical results. All authors wrote, reviewed and approved the manuscript.

Additional information

Supplementary Information accompanies this paper at http://www.nature.com/scientificreports

The authors declare no competing financial interests.

How to cite this article: Meloni, S. *et al*. Modeling human mobility responses to the large-scale spreading of infectious diseases. *Sci. Rep.* **1**, 62; DOI:10.1038/srep00062 (2011).

Supplementary Information
Modeling human mobility responses to the large-scale spreading of infectious diseases

Sandro Meloni, Nicola Perra, Alex Arenas, Sergio Gómez,
Yamir Moreno and Alessandro Vespignani

July 4, 2011

Contents

1 Networks analysis **3**

2 Global invasion threshold in metapopulation networks with origin-destination diffusion **4**
2.1 Comparison with numerical results 8
2.2 Size dependency analysis 8

3 Behavioral changes **11**
3.1 Departure probability 11
3.2 Rerouting 12
3.3 Subpopulations affected by an outbreak as a function of R_0 when the rerouting mechanism is active 13
3.4 Results 15

4 Model's Implementation **16**
4.1 Internal nodes' dynamics 16
4.2 Numerical simulations 18

5 Sensitivity Analysis **18**
5.1 Effects of recovery rate μ 19
5.2 Effects of the parameter τ accounting for the time spent at destination 19
5.3 Effects of the mobility rate of infected individuals λ^I 19
5.4 Effects of rerouting intensity h 19
5.5 Effects of latency rate γ in SEIR model 19

Metapolulation models are a relevant framework to model spreading of infectious diseases between fragmented but coupled subpopulations. Each of these subpopulations is represented as a node in a network with a certain number of connections with others. Individuals diffuse following the paths defined by the links that connect subpopulations. Inside each subpopulation, individuals are assumed to be well-mixed, so that the evolution of the epidemic is determined by the reproductive number R_0 of the disease. In metapopulation systems this quantity is not sufficient to understand if a macroscopic fraction of subpopulations will experience an outbreak. The diffusion and coupling between each node must be considered. Using these arguments a new quantity is introduced: the global invasion threshold. This is in general a function of the basic reproductive number, the connectivity patterns, diffusion rates and mobility patterns. Recently, analytical solutions have been found for Markovian diffusion processes [1]. In this paper we consider a more realistic scenario for individuals' mobility. People have a home, and when they travel, they also go to a specific, not random destination [2].

In our study, we have first analytically evaluated the global invasion threshold for synthetic networks considering explicitly origin and destination matrices. We next added even more realism considering real networks, namely, the worldwide air transportation network, and different mechanisms that account for self-initiated behavioral changes that are induced by the spreading of the epidemic among different subpopulations. In doing so, we have focused on spontaneous behavioral changes due the evolution and awareness of the epidemic. For instance, when an epidemic outbreak takes place, people might minimize their contacts as a way to reduce the risk to get sick. Besides, it has also been documented that one of the most common risk aversion strategies consists of staying at home, i.e., not to engage in a travel if there is the perception (or certainty) that at destination the number of infected individuals is high. Another behavioral reaction is encountered when travels are not cancelled, but individuals decide instead to change their itinerary avoiding places in which the epidemic incidence is perceived as high. These two possible risk aversion scenarios are considered in our study through the implementation of two mechanisms accounting for such behavioral changes in a metapopulation framework. In this supplementary information, we give more details of the results presented in the main text. In particular, we first describe in details the synthetic and real world networks used in the analysis. Then we present the analytical derivation of the global invasion threshold with a simple non-markovian diffusion scheme with mobility patterns given by origins and destinations. Finally, we move to the numerical details and sensitivity analysis of the model in which real networks and behavioral changes are introduced.

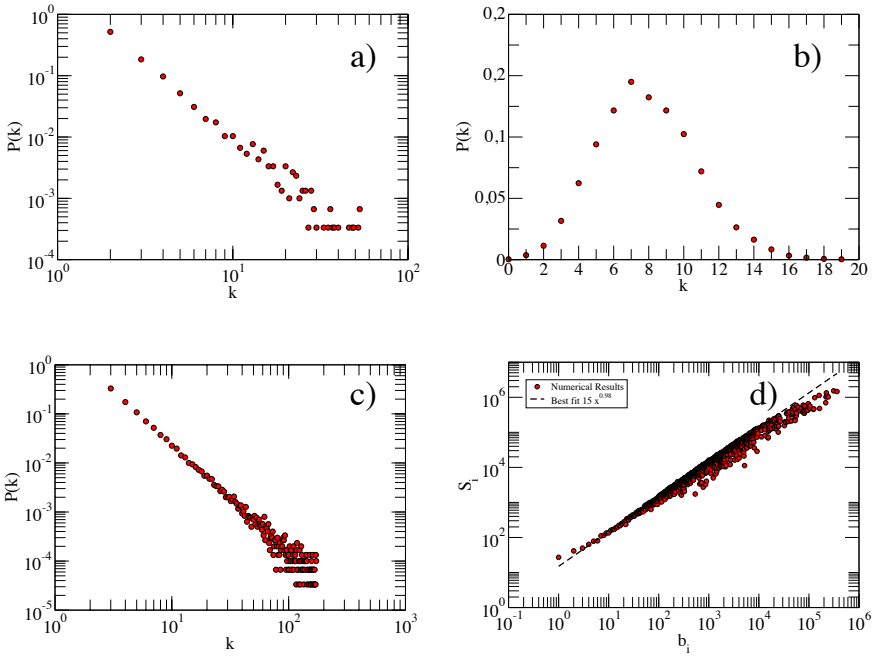

Figure 1: Degree distributions of the generated synthetic networks and correlations between nodes strength and betweenness centrality in the ATN. (a) Degree distribution $P(k)$ of the uncorrelated scale free network made up of $N = 3 \cdot 10^3$ subpopulations used as a substrate in our analysis. (b) Degree distribution $P(k)$ of a random network generated using the Erdös and Rényi model. The network is of the same size and average degree of that depicted in panel (a). (c) Degree distribution $P(k)$ of the uncorrelated scale free network with $N = 3 \cdot 10^4$ subpopulations used in the size dependency analysis. (d) Correlation between the observed traffic strength s_i of each node i in the ATN and the betweenness centrality values b_i produced by a the shortest path routing algorithm assumed in the simulations.

1 Networks analysis

Before starting our analysis let us present the networks we used as substrate to simulate real world populations. First, we focus on synthetic uncorrelated scale free networks that offer a controlled test-bench for the analytical treatment of the model and then we move to a realistic scenario considering the so-called Air Transportation Network (ATN). Synthetic scale free networks were generated following the recipe in [3]. In order to resemble as much as possible the ATN, we use a network of similar size $N = 3 \cdot 10^3$. One might argue that

this is a too short network size, as it is well-known that the Mean-Field approximation in quenched networks is valid for very large systems sizes. For finite networks, finite-size corrections might be needed.

Our results show that for a synthetic system of a size equivalent to that of the ATN, the analytical results nicely fit numerical simulations. This is because for $N = 3 \cdot 10^3$, the differences between homogeneous and heterogeneous networks already manifest (see Fig. 1a and Fig.1b). However, in order to test the effects of the network size in the results shown below, we have also built a larger scale free network made up of $N = 3 \cdot 10^4$ subpopulations. Figure 1c depicts the corresponding degree distribution.

Another assumption of our model that is related to the connection between synthetic and real networks has to do with the way individuals move through the networks. Specifically, we assume that individuals move from their home to the destination following the shortest path connecting them. In Fig.1d, we compare the observed nodes' strengths s_i from the ATN (i.e., real fluxes between any two given nodes) and the betweenness centrality b_i of that i when a shortest path routing algorithm is implemented. The linear association between the two sets of data doubtlessly indicate that the latter is indeed a quite good proxy for individual mobility.

2 Global invasion threshold in metapopulation networks with origin-destination diffusion

Let us consider a network $\mathbf{G}(V, M)$ with V nodes, M links and degree distribution $P(k)$. Each node i of the network is considered a subpopulation with N_i individuals. We set the subpopulation size proportional to its degree. Next, assume a diffusion process in which each individual in a node i (origin) travel to another node j (destination) of the network with a probability λ. The destination choice j is selected with a probability proportional to the subpopulation size N_j. Once individuals engage in a travel, the shortest path is selected among all the possible paths connecting the origin and the destination of the travel. Besides, we also consider that individuals come back to their home subpopulations after they reach their destinations. A standard convenient representation of the system is provided by quantities defined in terms of the degree k:

$$N_k = \frac{1}{V_k} \sum_{i|k_i=k} N_i. \tag{1}$$

Let us consider that an individual of a subpopulation of degree k gets some infectious disease characterized by a reproductive number $R_0 > 1$. Let us define D_k^0 as the number of diseased subpopulations of degree k at generation 0. In the early stage, the number of diseased subpopulations is small, thus, we can study the evolution of this number using a tree-like approximation (where no correlations are considered) relating D_k^n with D_k^{n-1}. The average number of infected individuals in the class of degree k during the evolution of the epidemic

is αN_k. The parameter α depends on the specific disease. Each infected individual stays in the infectious state for an average time μ^{-1}. Then the number of infected people circulating through the network after $n-1$ generations is:

$$\omega^{n-1} = \frac{\lambda\alpha}{\mu} \sum_{k'} D_{k'}^{n-1} N_{k'} \tag{2}$$

The number of infected individuals that will pass through a subpopulation of degree k will be a fraction of Eq. (2) proportional to the topological betweenness (in general, it is proportional to the algorithmic betweenness, but given that individuals are following the shortest path, it coincides with the topological one in our case). This measure is defined as:

$$b(i) = \sum_{\substack{j,l=1,n \\ i\neq j\neq l}} \frac{\mathcal{D}_{jl}(i)}{\mathcal{D}_{jl}}, \tag{3}$$

where $\mathcal{D}_{jl}$ is the total number of shortest paths from j to l and $\mathcal{D}_{jl}(i)$ is the number of shortest paths from j to l that goes through i. The latter quantity also measures the centrality of a node assuming a diffusion scenario in which travelers go through the shortest paths. We can then write:

$$\gamma_k^{n-1} = \frac{b_k}{b_{tot}} \omega^{n-1}, \tag{4}$$

where b_{tot} is the sum of all the betweenness of the nodes. For the n^{th} generation we have:

$$D_k^n = V_k \left(1 - \frac{D_k^{n-1}}{V_k}\right) \left[1 - R_0^{-\gamma_k^{n-1}}\right], \tag{5}$$

where the second factor on the right is the probability that the subpopulation is not already seeded by infected individuals and the last is the probability that the new seeded subpopulation will experience an outbreak. In the early time and for $R_0 \sim 1$ we can approximate the last expression considering:

$$\frac{D_k^{n-1}}{V_k} << 1, \tag{6}$$

and

$$1 - R_0^{-\gamma_k^{n-1}} \sim (R_0 - 1)\gamma_k^{n-1}, \tag{7}$$

obtaining:

$$D_k^n = (R_0 - 1) V_k \gamma_k^{n-1} = (R_0 - 1) \frac{\lambda\alpha}{\mu} V_k \frac{b_k}{b_{tot}} \sum_{k'} D_{k'}^{n-1} N_{k'}. \tag{8}$$

Considering at the equilibrium:

$$N_k = \frac{k}{\langle k \rangle} \bar{N}, \tag{9}$$

where $\bar{N} = \sum_k P(k)N_k$ is the average subpopulation size, we get:

$$D_k^n = (R_0 - 1)\frac{\lambda\alpha}{\mu}\bar{N}V_k\frac{b_k}{b_{tot}}\frac{1}{\langle k\rangle}\sum_{k'} D_{k'}^{n-1}k'. \tag{10}$$

Let us define now $\Theta^n = \sum_k D_k^n k$, then we have:

$$\Theta^n = (R_0 - 1)\frac{\lambda\alpha}{\mu}\bar{N}\frac{\Theta^{n-1}}{\langle k\rangle}\sum_k V_k k\frac{b_k}{b_{tot}}. \tag{11}$$

The last term needs can be further developed as:

$$\sum_k V_k k\frac{b_k}{b_{tot}} = \frac{V\sum_k P(k)kb_k}{V\sum_{k'} P(k')b_{k'}}. \tag{12}$$

Considering now $b_k \sim k^\eta$ one is left with:

$$\Theta^n = (R_0 - 1)\frac{\lambda\alpha}{\mu}\bar{N}\frac{1}{\langle k\rangle}\frac{\langle k^{1+\eta}\rangle}{\langle k^\eta\rangle}\Theta^{n-1}. \tag{13}$$

We finally get the global invasion threshold as:

$$R^* = (R_0 - 1)\frac{\lambda\alpha}{\mu}\bar{N}\frac{1}{\langle k\rangle}\frac{\langle k^{1+\eta}\rangle}{\langle k^\eta\rangle}. \tag{14}$$

We can write the threshold condition for the mobility rate:

$$\lambda\bar{N} \geq \frac{\langle k^\eta\rangle}{\langle k^{1+\eta}\rangle}\frac{\langle k\rangle\mu}{\alpha}(R_0 - 1)^{-1}. \tag{15}$$

These last two expressions are the crucial quantities, and give the conditions for a global outbreak. It is important to remind that in metapopulation networks the condition $R_0 > 1$ for each subpopulation is not enough to infer whether a finite number of subpopulations will be affected by the disease. The diffusion process must be considered, and it defines the form and value of the invasion threshold. The previous arguments are valid for the case in which:

$$\mu^{-1} \gg \bar{l}v^{-1}, \tag{16}$$

where $\bar{l}$ is the average distance between nodes and v^{-1} is the traveling *speed* of individuals that we set as 1 node per time step. In other words, this means that sick individuals are infectious for a large enough time compared with the time it takes for individuals to complete their travel. This is a necessary condition for Eq. (4) to be valid. We can easily get an expression in the other limit:

$$\mu^{-1} \ll \bar{l}v^{-1}, \tag{17}$$

in this case each individual will be infectious for a time window smaller enough as to infect only the nearest neighbors. In this case the spreading can be thought

of as a Markovian process and all the analytics is the same reported in Ref. [1]. The expression for the number of infected nodes at the n^{th} generation will be then:

$$D_k^n = \sum_{k'} D_{k'}^{n-1}(k'-1)\left[1 - R_0^{-\lambda_{k'k}}\right] P(k|k')\left(1 - \frac{D_k^{n-1}}{V_k}\right), \tag{18}$$

using the usual approximations (6), (7) and assuming that degree correlations can be neglected we have:

$$D_k^n = \frac{(R_0-1)}{\langle k\rangle} kP(k) \sum_{k'} D_{k'}^{n-1}(k'-1)\lambda_{k'k}. \tag{19}$$

Considering an homogeneous diffusion we can write:

$$\lambda_{k'k} = \frac{\lambda}{k'}\frac{\alpha N_{k'}}{\mu}, \tag{20}$$

where $N_{k'} = \frac{k'}{\langle k\rangle}\bar{N}$. Using this expression we get:

$$D_k^n = \frac{\lambda\alpha}{\mu}\frac{(R_0-1)\bar{N}}{\langle k\rangle^2} kP(k) \sum_{k'} D_{k'}^{n-1}(k'-1). \tag{21}$$

Let us defined $\Theta^n = \sum_k D_k^n(k-1)$, after multiplying both sides for $(k-1)$ and after summing over all k we get:

$$\Theta^n = \frac{\lambda\alpha}{\mu}\frac{(R_0-1)\bar{N}}{\langle k\rangle^2}\Theta^{n-1} \sum_k k(k-1)P(k), \tag{22}$$

or

$$\Theta^n = \frac{\lambda\alpha}{\mu}\frac{(R_0-1)\bar{N}}{\langle k\rangle^2}\Theta^{n-1}(\langle k^2\rangle - \langle k\rangle). \tag{23}$$

We finally got an expression for the global invasion threshold:

$$R^* = \frac{\lambda\alpha}{\mu}(R_0-1)\bar{N}\frac{\langle k^2\rangle - \langle k\rangle}{\langle k\rangle^2}, \tag{24}$$

and for the mobility rate

$$\lambda\bar{N} \geq \frac{\mu}{\alpha(R_0-1)}\frac{\langle k\rangle^2}{\langle k^2\rangle - \langle k\rangle}. \tag{25}$$

2.1 Comparison with numerical results

To compare the analytical approach with the numerical results we choose as substrate an uncorrelated scale free network generated according to the uncorrelated configuration model with $\gamma = 2.5$ and $N = 3000$. First of all we tested the assumption made in Eq. (9), in which the number of individuals N_k at nodes of degree k, at the equilibrium, is proportional to k. To do so, we start the simulation with a population of $N_i \simeq 1000$ in each node, wait until the traffic equilibrium has been reached, and finally we collect the values of N_i. Fig. (2)a shows the values of N_k as function of degree k, justifying our assumption. In order to calculate the critical mobility rate λ_c we use Eq. (15) and λ_c reads as:

$$\lambda_c = \frac{1}{\bar{N}} \frac{\langle k^\eta \rangle}{\langle k^{1+\eta} \rangle} \frac{\langle k \rangle \mu}{\alpha} (R_0 - 1)^{-1}. \tag{26}$$

Thus, we need to know the specific value of η in the chosen network and fix a value for R_0. To obtain an estimate for η we compute the value of the betweenness b_i for each node i and coarse grain it by degree classes k as,

$$b_k = \frac{1}{V_k} \sum_{i|k_i=k} b_i. \tag{27}$$

Note that to evaluate b_i of each node we decide to make a run of the simulation and register the number of packets that pass through a link over a very long period of time. In this way, the values of b_i are more precise and closer to the actual dynamics. Fig. (2)b shows b_k as function of the degree classes and the fit for η gives a value of $\eta = 1.51$.

Now we have all the ingredients to calculate the critical value λ_c and compare it with the numerical results. First we calculate the mean degree of the network $\langle k \rangle = 4.0$ and then the η^{th} moment of the degree distribution obtaining $\langle k^\eta \rangle = 10.93$ and finally the $(1+\eta)^{th}$ moment $\langle k^{1+\eta} \rangle = 158.60$. Considering $R_0 = 1.5$ and that $\bar{N} = 1000$, and substituting α in Eq. (26) one gets

$$\lambda_c = \frac{1}{\bar{N}} \frac{\langle k^\eta \rangle}{\langle k^{1+\eta} \rangle} \frac{\langle k \rangle \mu R_0^2}{2(R_0 - 1)^2} = \frac{1}{1000} \frac{10.93}{158} 4.0 \cdot 0.04 \cdot \frac{1.5^2}{2 \cdot 0.5^2} = 0.0000496. \tag{28}$$

In Fig. 2c we show the good agreement obtained when comparing the numerical simulations of the model and the analytical prediction for the global invasion threshold. Besides, a similar calculation but for $\mu = 0.5$ gives the second limit Eq. (17), which is compared in Fig. 2d with numerical simulations, showing again a good agreement.

2.2 Size dependency analysis

As previously argued, one would expect finite size corrections to the Mean-Field approach for small systems. In order to address this issue, we consider a larger synthetic scale free network made up of $N = 3 \cdot 10^4$ nodes. Also for this

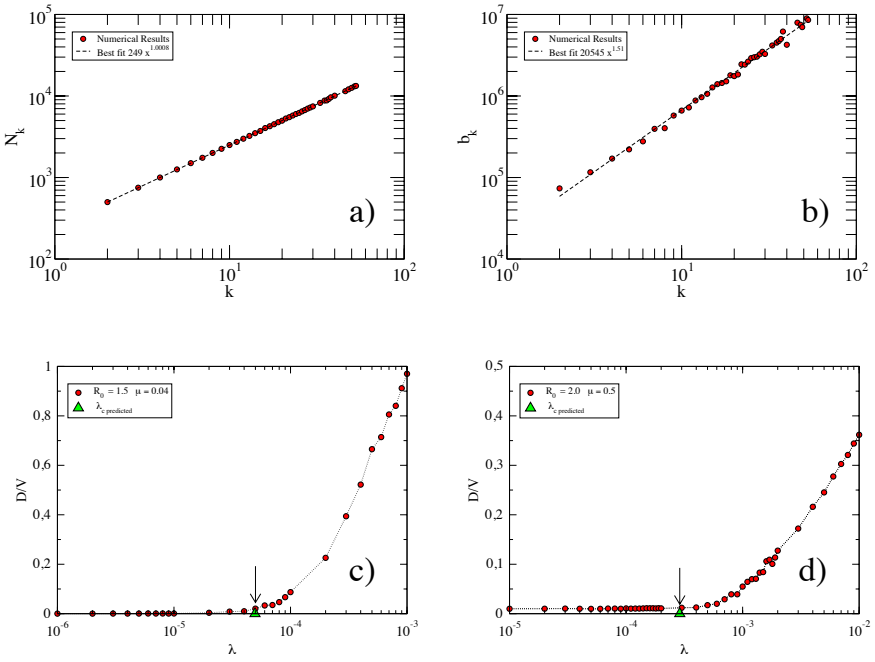

Figure 2: Panel (a) represents N_k as a function of the degree classes k and the best fit, which leads to a linear scaling. In panel (b), we show b_k as a function of the degree classes k and the best estimated value for η is 1.51. In panels (c) and (d), we show the fraction of infected subpopulations in the null model as a function of the mobility rate λ for two different values of μ such that $\mu^{-1} \gg \bar{l}v^{-1}$ (c) and $\mu^{-1} \ll \bar{l}$ (d).

case we have checked the assumption made in Eq. 9 and estimated the value of η from the relation between k and b_k. In Fig. 3a we show the scaling between the population on nodes of degree k and k. Again, the scaling turns out to be linear. Moreover, Fig.3b represents the dependency of b_k with k, from which a value of $\eta = 1.161$ is obtained.

We have also tested the robustness of our derivation when infected individuals move at a lower rate than other individuals, which is a realistic ingredient. In this case we simply need a rescaling of Eq. 26. If, for simplicity, we assume $\lambda^I = \lambda/2$ we obtain:

$$\lambda_c = \frac{2}{\bar{N}} \frac{\langle k^\eta \rangle}{\langle k^{1+\eta} \rangle} \frac{\langle k \rangle \mu}{\alpha} (R_0 - 1)^{-1}. \tag{29}$$

Now considering the mean sub-population size $\bar{N} = 1000$ and $R_0 = 1.5$ we can

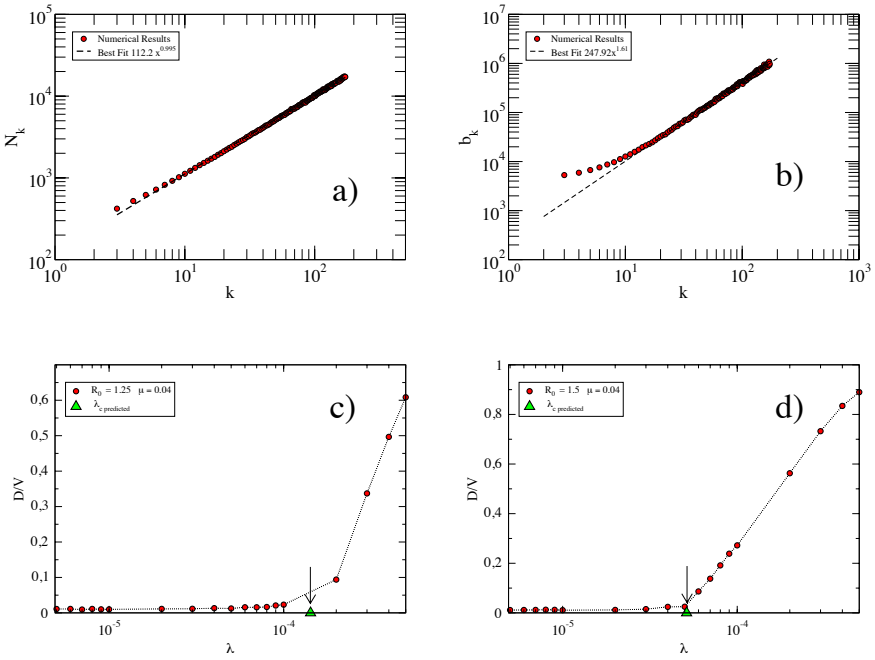

Figure 3: Panel (a) represents N_k as a function of the degree classes k. The best fit leads to a linear scaling for the $N = 3 \cdot 10^4$ uncorrelated scale free network. In panel (b), we show b_k as a function of the degree classes k, from which a best estimate gives $\eta = 1.51$. Panels (c) and (d) depict the fraction of infected subpopulations in the null model as a function of the mobility rate λ for two different values of R_0, $R_0 = 1.25$ (c) and $R_0 = 1.5$ (d).

calculate the invasion threshold value as:

$$\lambda_c = \frac{2}{\bar{N}} \frac{\langle k^{\eta} \rangle}{\langle k^{1+\eta} \rangle} \frac{\langle k \rangle \mu R_0^2}{2(R_0 - 1)^2} = \frac{2}{1000} \frac{61.91}{3817.69} 8.78 \cdot 0.04 \cdot \frac{1.5^2}{2 \cdot 0.5^2} = 0.0000513068. \tag{30}$$

Figures. 3c and 3d show that also in this case we get a good agreement between numerical simulations and the analytical prediction.

3 Behavioral changes

During the evolution of an infectious disease, one usually finds that due to risk perception, people change their traveling habits. Individuals can decide to stay at home, to avoid crowded places, to reschedule trips, holidays etc.. All realistic epidemic models are based on structured data of human activities [5, 6, 7]. During catastrophic events the system can be driven out of equilibrium invalidating the predictive power of existing models. Therefore, behavioral changes should be in principle considered in any realistic attempt to model the dynamics of global infectious diseases. In the recent literature, a few attempts to model behavioral changes have been done [8, 9, 10, 11, 12, 13, 14] but any of these tackle the effect of social disruption inside a metapopulation framework. Motivated by this, we introduce different mechanisms that might model spontaneous self-initiated behavioral responses to the presence of a disease. In our full model with such changes incorporated, origin-destination matrices are still considered. Furthermore, with the aim of being more realistic, we use in our simulations the worldwide air transportation network in which each node/subpopulation i represents an airport and for each connected pair (i, j) a weight ω_{ij} (number of passengers in that route) is assigned. The number of individuals in each subpopulation is set proportional to the strength:

$$N_i = \sum_j \omega_{i,j}. \tag{31}$$

As we have discussed in the previous sections, each individual will chose the destination among all possible subpopulations with a probability that is proportional to the subpopulations sizes. In this way the known heterogeneity of the traffic is explicitly considered. Let us now imagine that an individual from node i selects as destination subpopulation j and let d_{ij} be the traveled distance in terms of hops needed to reach the chosen destination. In the previous model we assumed that once the destination is reached, each individual goes back immediately. Instead in this second more realistic implementation we assume that each traveler stay τ time steps at destination. We extract the waiting times τ from a uniform distribution with mean d_{ij}, so that the longer the trip, the larger the stay. Moreover, we also assume that the probability that an infected individual will travel is half of the same quantity for healthy people, as infected people once aware of the illness usually refrain from traveling. These elements constitute all together the new baseline of our model. In the next sections we describe the different mechanisms we use to model behavioral changes.

3.1 Departure probability

During the H1N1 pandemic in 2009, especially in the early stage, a big drop in the number of travelers to (and within) Mexico was registered [15]. A first plausible mechanism to model behavioral changes is obtained changing the probability of departure according to the stage of the disease at a given destination. We can thus assume that individuals might decide to postpone their

trips. Mathematically this behavior can be modeled as:

$$\lambda \to \lambda_{ij} = \lambda \left[1 - \frac{I_j(t)}{N_j(t)} \right]. \tag{32}$$

The expression above considers that the probability that each individual will travel is not anymore constant but a function of the epidemic incidence at destination. At the beginning of the spreading process, when the number of infected individuals is small, the mobility is given by λ for all possible destinations j, since the second factor above is close or equal to 1. However, during the evolution of the disease, as soon as the number of infected individuals increases, the departure probability starts to change from place to place and the mechanism becomes effective.

3.2 Rerouting

Let us assume that a traveler from subpopulation i has as destination subpopulation j, and that a node m is in the shortest path between its origin and destination. Let us also suppose that subpopulation m is experiencing a severe outbreak. The individual could decide to travel anyway but changes the route going through another, maybe longer but less risky alternative path. We modeled this kind of behavior by introducing a cost function:

$$c_m(t) = h\delta_m + (1-h)\frac{I_m(t)}{N_m(t)}, \tag{33}$$

where the parameter h is defined in the closed interval $[0, 1]$ and δ_k can assume three values $[-1, 0, 1]$. -1 is associated to the shortest path (the individual will be one hop closer to its destination), 0 to a new path which does not change the current distance to the destination, and 1 otherwise (the individual will be one hop farther to its destination). At each time step, each individual that is traveling decides the next node to move to by minimizing the cost function Eq. (33), unless the next move leads to its destination. Other functional forms for Eq. (33) could also be defined, however, Eq. (33) is a simple proxy for an stochastic choice based on the minimum information available.

It is worth noticing that the parameter h, although defined in the interval $[0, 1]$ can take on only a small subset of meaningful values. If h is too small, the traveler essentially moves through the network following the landscape of epidemic incidence, as no information of its destination is taken into account when deciding where to move. This is a highly unrealistic situation that therefore sets a lower bound (> 0) to h. Similarly, one can easily show that h is also bounded from above. Although $h = 1$ mathematically corresponds to the limit of shortest path, this limit is obtained well before. Admittedly, one can show that in order for a traveler to go through a path one hop farther than the destination the following condition must be satisfied

$$\frac{I_-(t)}{N_-(t)} - \frac{I_+(t)}{N_+(t)} > \frac{2h}{1-h}, \tag{34}$$

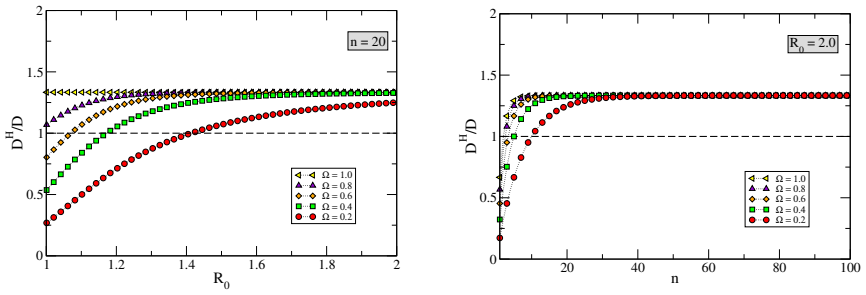

Figure 4: Numerical solution of the ratio between the number of diseased subpopulation with and without rerouting, Eq. (39), for different values of n, R_0 and Ω as indicated in the panels. The other parameters have been set to $l = 3$ and $\Delta l = 1$. The lines are a guide to the eye and mark the values of R_0 and n at which the crossover takes place.

where $\frac{I_-}{N_-}$ and $\frac{I_+}{N_+}$ are the densities of infected individuals at subpopulations one hop closer and one hop farther from the traveler's destination, respectively. The same argument leads to the following condition with respect to the possibility of going through a path that does not change the current distance to destination:

$$\frac{I_-(t)}{N_-(t)} - \frac{I_=(t)}{N_=(t)} > \frac{h}{1-h}, \tag{35}$$

where $\frac{I_=}{N_=}$ is the density of infected individuals at a subpopulation which is at the same distance of the traveler's destination. We have checked that our results for the model including behavioral changes are qualitatively the same for different values of h in the interval $[0.05, 0.2]$ (beyond $h = 1/3$, no differences with respect to the shortest path results are obtained, which means that this limit has been reached at $h = 1/3$ as expected from Eq. (34)).

3.3 Subpopulations affected by an outbreak as a function of R_0 when the rerouting mechanism is active

When the h mechanism is active, the number of individuals going through a node in the shortest path between an origin and a destination decreases due to the rerouting of individuals induced by the risk aversion mechanism. This implies that a smaller number of individuals goes through that node. This mechanism defines an interesting phenomenology whose effect on the number of diseased subpopulations is non-linear and depending on the reproductive number R_0 and the number of traveling individuals n.

Let us consider that $n(\lambda)$ traveling individuals starts at subpopulation i with destination in the subpopulation j. Besides, consider that one node r in

the path connecting both subpopulations is infected. In the case without any behavioral responses the shortest path is selected and let us consider its length as l. The number of new diseased subpopulations on the way will be:

$$D^{new} = l(1 - R_0^{-n}), \tag{36}$$

assuming for now that the $l - 1$ subpopulations in the shortest path are not already diseased. Instead, in the case in which the re-routing mechanism to avoid infected subpopulations is active, individuals may go through alternative paths. Thus, we will have that:

$$D_{RR}^{new} = (l + \Delta l)(1 - R_0^{-n\Omega}) \tag{37}$$

where Ω, $0 < \Omega \leq 1$ represents the ratio of infected individuals that have been rerouted. If all the $k - 1$ neighbors of the nodes before r are not diseased we can evaluate

$$\Omega \sim \frac{1}{k-1} \tag{38}$$

Then, we take the ratio among the two quantities yielding

$$\frac{D_{RR}^{new}}{D^{new}} = \frac{(l + \Delta l)(1 - R_0^{-n\Omega})}{l(1 - R_0^{-n})}. \tag{39}$$

By expanding both the numerator and denominator for $R_0^{-n} \sim 1$, Eq. (39) can be written as

$$\frac{D_{RR}^{new}}{D^{new}} \sim (1 + \frac{\Delta l}{l})\Omega. \tag{40}$$

As Ω is of order $1/k$ (in the best case scenario one does not expect multiple change of paths), and Δl and l can be considered to be of the same order, we can expect

$$\frac{D_{RR}^{new}}{D^{new}} < 1, \tag{41}$$

The previous expression has been obtained for $R_0 \sim 1$ and n relatively small. For large R_0 and n values, we are in a different regime in which the probabilities $\left[1 - R_0^{-n}\right]$ 1 and $\left[1 - R_0^{-n\Omega}\right]$ 1 are independent of Ω thus defining

$$\frac{D_{RR}^{new}}{D^{new}} > 1. \tag{42}$$

Therefore, we expect a crossover from $D_{RR}^{new}/D^{new} < 1$ to $D_{RR}^{new}/D^{new} > 1$ in R_0 and n. As n is an increasing function of the diffusion rate λ, the crossover is observed also for increasing values of this parameter. We plot the behavior of Eq. (39) in Fig. 4 for different values of n, R_0 and Ω, setting $l = 3$ and $\Delta l = 1$ (plausible values in any random or complex networks) which confirms our findings from mechanistic numerical simulations discussed in the main text.

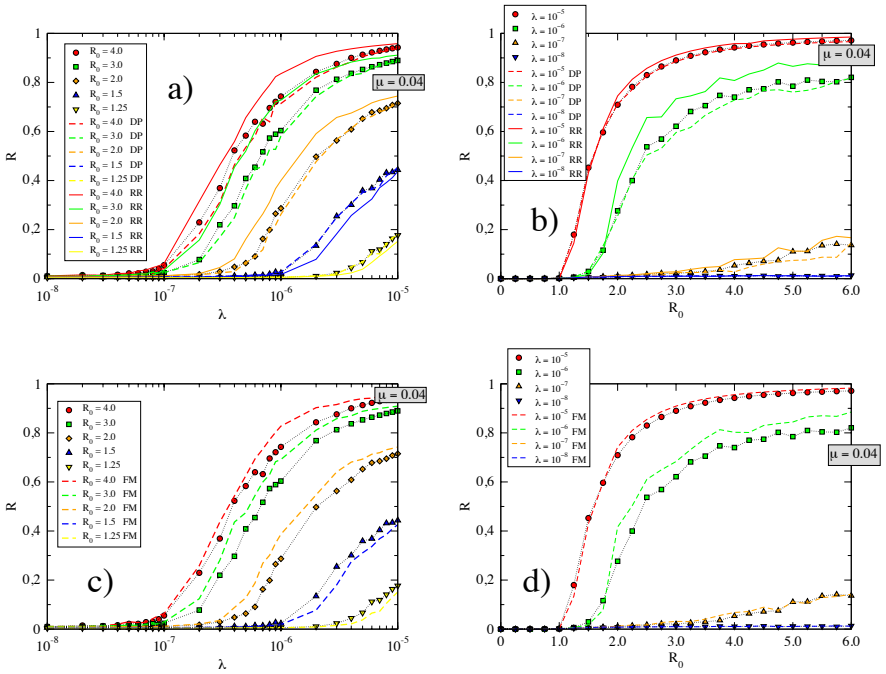

Figure 5: Comparison between the fraction of infected individuals R obtained for the baseline model (i.e., when no behavioral changes are implemented) with that obtained with different risk aversion mechanisms as a function of R_0 or λ. Panels (a) and (b) show the results when the departure probability (DP) and the rerouting (RR) mechanisms are switched on separately. Panels (c) and (d) represent the same quantity but using the full model defined in the text. We have fixed $\mu = 0.04$. The underlying network is the worldwide air transportation network (see the text for further details).

3.4 Results

In this section we discuss the results obtained by implementing separately the two proposed mechanisms and when both are combined into a single, full model. We first notice that the critical invasion threshold λ_c is the same for all the variants of the model. This critical point is independent of the behavioral changes because the model dynamics does not change at low values of the epidemic incidence, i.e., just around the global invasion threshold. In Fig. (5) we show the ratio of infected individuals R (epidemic size) as a function of λ (panel (a)) and R_0 (panel(b)). In the main text of the paper we show the same type of plots done instead for the ratio of diseased subpopulations D/V. The three different implementations of the model are shown as indicated in the legends: the baseline, the departure probability mechanism (DP) and the

rerouting mechanism (RR).

Departure probability

This mechanism brings a smaller reduction of the epidemic size for large values of R_0. In the other case instead the mechanism is not distinguishable from the baseline. This is due to the fact that for mild epidemics the number of infected individuals is small and then we can consider $\lambda_{ij} \sim \lambda$. Our results confirm previous findings about the inefficacy of measures like cutting down mobility of individuals by, for instance, closing airports [16, 17, 18, 19].

Rerouting

This mechanism brings, for values of λ consistently bigger than its critical value, a bigger epidemic size with respect to the baseline model. This is due to the fact that, trying to minimize the risks to get sick, individuals change their route visiting places that otherwise would have not been visited, therefore contributing to a wider spread of the disease. As discussed in the preceding section, the previous behavior is not always obtained, since for low values of R_0 the number of individuals going through a node in the shortest path between an origin and a destination decreases due to the rerouting of individuals induced by the risk aversion mechanism. This is what happens, for instance, for $R_0 = 1.25$ and $R_0 = 1.5$ in Fig. (5)a and Fig. (5)b.

Full model

We implemented both mechanisms together in a full version of the model. As shown in Fig. (5)c and Fig. (5)d the effect of both risk aversion mechanisms on the epidemic size depends on the value of R_0 and λ. For $R_0 \geq 2$ and values of λ larger than the global invasion threshold the full model leads to a bigger epidemic size when compared to the baseline implementation. In these regions of parameters, the rerouting mechanism is the dominant one and the large outbreak is due to the fact that people explore much more the network trying to minimize their risk to get sick. This self-fish strategy gives a worst scenario confirming how behavioral changes have a significant impact on the invasion dynamics in a non trivial way.

4 Model's Implementation

4.1 Internal nodes' dynamics

In each node a SIR dynamics takes place over a well mixed population of initial size $N_i(0) = w_i$, being w_i the strength of node i. When time goes on, $N_i(t)$ changes according to the number of individuals that has been received and has left the node. Within the nodes, one step of a SIR process takes place. The

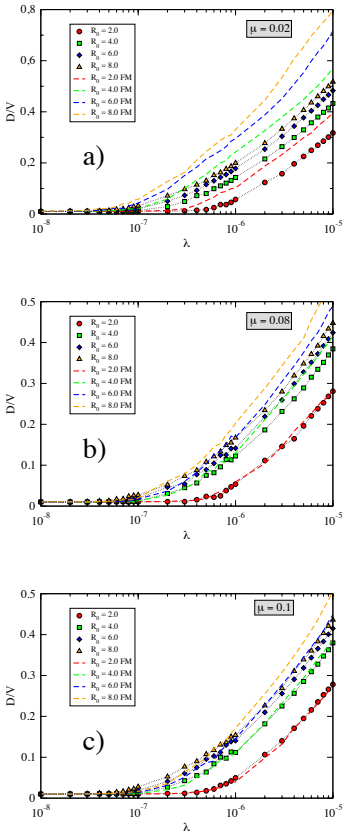

Figure 6: Comparison between the number of subpopulations affected by the outbreak, D/V, in the full ($\tau = 1$ and $\lambda^I = \lambda/2$) and null versions of the model for $\mu = 0.02, 0.08$ and 0.1 as indicated. The network is the Air Transportation Network and destinations are chosen proportionally to nodes' strengths.

state of every individual inside a node i is changed according to the following probabilities: a susceptible individual becomes infected with probability $p^{(S\to I)} = 1 - (1 - \frac{\beta}{N_i})^{I_i}$, and an infected recovers with probability $p^{(I\to R)} = \mu$. Specifically, the exact number of individuals that changes its state is determined by a binomial distribution with the probability $p^{(S\to I)}$ (or $p^{(I\to R)}$) and the susceptible populations size $S_i(t)$ (or infected $I_i(t)$) as parameters. Note that in this scenario, R_0 only participates in the internal dynamics; individuals traveling through node i are involved in the SIR and thus can change their state while at node i.

Parameter	Range explored
μ	$0.02 - 0.1$
τ	$\tau/3 - 3\tau$
λ^I	$\lambda/4 - \lambda$
h	0.05−1.0
γ	$1/4 - 1$

Table 1: Summary of the sensitivity analysis performed.

4.2 Numerical simulations

The model is implemented as follows. Each simulation starts with a small number of infected individuals (1% of the individuals is infected within a randomly chosen subpopulation). In the simulations the traffic and spreading dynamics have the same time scale so, at each time step, first a diffusion step is performed and then the SIR internal dynamics is evaluated. For the diffusion of the individuals, we assume that the number of individuals starting a trip at time t is given by a binomial distribution with the mobility rate λ and the subpopulation size $N_i(t)$ as parameters. Destinations are chosen according to the population w_i of each node. To keep the nodes' population constant over time (excluding transient individuals traveling through the node), once an individual reaches its destination it starts a new trip back to its origin. Simulations run until $I(t) = 0$ for all subpopulations. Note that in this framework only travelers are explicitly followed and that we only keep a counter for the number of non-traveling individuals inside each node.

5 Sensitivity Analysis

To test the sensitivity of our main results to different choices of the model parameters, we have performed further numerical simulations varying them. Namely, the dependency of the results presented throughout this work with the following parameters was explored: the recovery rate μ, the time spent at destination before travelling back home τ, the mobility rate of the individuals λ^I and the re-routing intensity h. As an additional test we also extend our model including a further class of exposed individuals in which the transition from exposed to infected is governed by the transition rate γ. Table 1 summarizes the sensitivity results shown in the following subsections. Up to the range explored, the conclusions of our study remain the same. We note that given the large number of parameters involved and the large computational times required by the simulations, the sensitivity analysis has been restricted to values of the parameters within the typical ranges of epidemiological models or reasonable assumptions as given by the phenomenology of the models discussed.

5.1 Effects of recovery rate μ

We have studied the model behavior for other three different values of μ. In Fig. 6 we compare the results of the full model with $\tau = 1$ and $\lambda^I = \lambda/2$ for $\mu = 0.02$(a), 0.08(b) and 0.1(c) and four different values of $R_0 = 2, 4, 6, 8$. The results show that the behavior of the full model with respect to the baseline case is qualitatively the same regardless of the specific value of μ.

5.2 Effects of the parameter τ accounting for the time spent at destination

In Fig. 7 we compare the results of the full model using three different values of τ: $\tau' = \tau/2$ (a), $\tau' = 2 \cdot \tau$ (b) and $\tau' = 3 \cdot \tau$ (c), respectively, with the baseline case. No qualitative change of behavior is observed with respect to the results in the main text.

5.3 Effects of the mobility rate of infected individuals λ^I

Fig. 8 shows the results of the full model for three different values of the mobility rate of infected individuals $\lambda^I = \lambda/4$ (a),$\lambda^I = \lambda/3$ (b) and $\lambda^I = \lambda$ (c). Results corresponding to $\lambda^I = \lambda/2$ are presented in the main text. Note that although the value of λ^I determines a variation on the global invasion threshold no qualitative change of behavior is observed with respect to the previous results. The network is the Air Transportation Network and destinations are chosen proportionally to nodes' strengths.

5.4 Effects of rerouting intensity h

We have studied the model behavior for a family of h values. As shown in Fig. 9, the full model always performs worse than the null case, provided that $h < 1/3$. When h is above this value, all the curves collapse into a single family, whose behavior is nearly the one observed when individuals move following the shortest path.

5.5 Effects of latency rate γ in SEIR model

Here we simulate an SEIR model assuming that individuals go from susceptible to exposed and then to the infected class at a rate γ. The latter is set to three different values $\gamma = 0.25$, 0.33 and 0.5 respectively. Fig. 10 shows that the addition of this new compartment does not alter the qualitative behavior of the model without such a class.

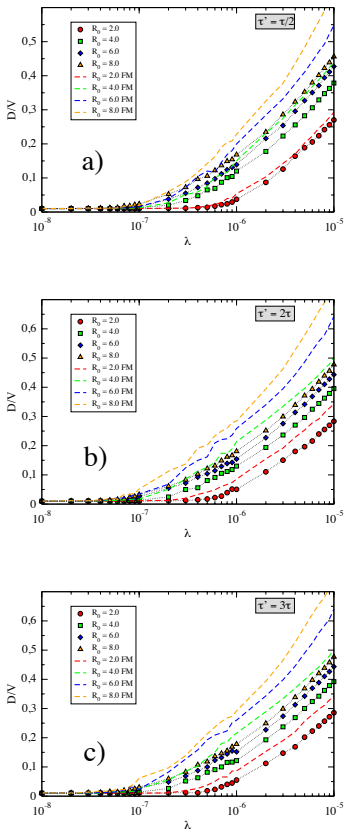

Figure 7: Comparison between the full and null versions of the model for $\mu = 0.04$ and three choices for the time spent at destination before traveling back home $\tau' = \tau/2, 2 \cdot \tau$ and $3 \cdot \tau$. D/V is the number of subpopulations affected by the outbreak. The network is the Air Transportation Network and destinations are chosen proportionally to nodes' strengths.

References

[1] Colizza V. Vespignani V. (2008). Epidemic modeling in metapopulation systems with heterogeneous coupling pattern: Theory and simulations, *J. Theor. Biol.* 251:450-467

[2] Meloni, S., Arenas, A., Moreno, Y. (2009) Traffic-driven epidemic spreading in finite-size scale-free networks. *Proc. Nat. Acad. Sci. USA* 106:16897-16902.

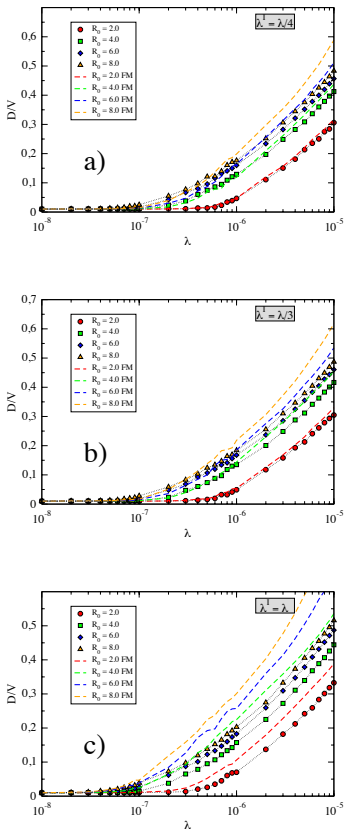

Figure 8: D/V in the full and null versions of the model for $\mu = 0.04$ and mobility rates of infected individuals, λ^I, as indicated in the figure. The network is the Air Transportation Network and destinations are chosen proportionally to nodes' strengths.

[3] Catanzaro, M., Boguña, M., Pastor-Satorras, R. (2005) Generation of uncorrelated random scale-free networks. *Phys. Rev. E* 71, 027103.

[4] Pastor-Satorras R., Vespignani A. (2001) Epidemic spreading in scale-free networks. *Phys. Rev. Lett.* 86:3200-3203.

[5] Ferguson N.M. (2007). Capturing Human Behaviour, *Nature*, 466:733

[6] Brockmann D. Hufnagel L. Geisel L. (2006). The scaling laws of human travel, *Nature* 439:462-465.

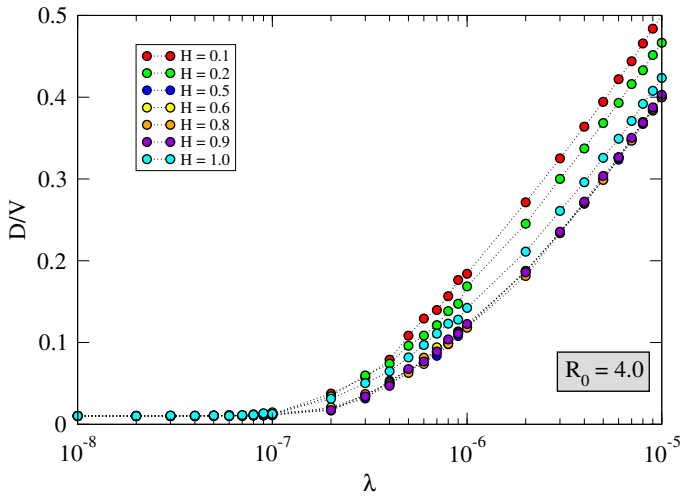

Figure 9: Results for D/V obtained using different values of h when the second risk aversion mechanism is active. The network is the Air Transportation Network and destinations are chosen proportionally to nodes' strengths.

[7] Balcan D. Colizza V. Goncalves B. Hu H. Ramasco J.J. Vespignani A. (2009). Multiscale mobility networks and the large scale spreading of infectious diseases, *Proc. Natl. Acad. Sci. USA*, 106:21484.

[8] Hatchett R.J., Mecher C.E., Lipsitch M (2007) Public Health Interventions and Epidemic Intensity During the 1918 Influenza Pandemic, *Proc. Natl. Acad. Sci. USA* 104:7582-7587.

[9] Bootsma M.C.J., Ferguson N.M. (2007) The Effect of Public Health Measures on the 1918 Influenza Pandemic, *Proc. Natl. Acad. Sci. USA* 104: 7588-7593.

[10] Markel H., Lipman H.B., Navarro J.A., Sloan A., Michalsen J.R., Stern A.M., Cetron M.S. (2007) Nonpharmaceutical Interventions Implemented by US Cities During the 1918-1919 Influenza Pandemic, JAMA, 298:2260.

[11] Goffman W., Newill V.A. (1964) Generalization of Epidemic Theory an Application to the Transmission of Ideas, *Nature*, 204:225-228.

[12] Poletti P., Caprile B., Ajelli M., Pugliese A., Merler S. (2009). Spontaneous Behavioural Changes in Response to Epidemics, *J. Theor. Biol.* 241:193204.

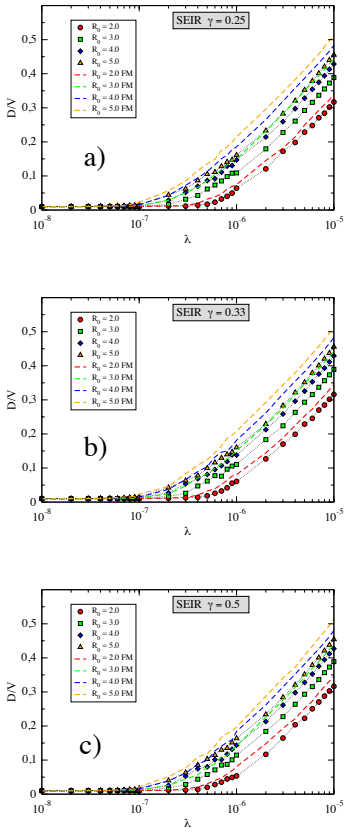

Figure 10: Comparison between the number of subpopulations affected by the outbreak, D/V, in the full and null versions of an extended model in which an exposed class has also been included. The transition from exposed to infected is set to $\gamma = 1/4$ (a), $\gamma = 1/3$ (b) and $\gamma = 1/2$ (c) , while the rest of parameters are $\mu = 0.04$, and $h = 0.1$. The network is the Air Transportation Network and destinations are chosen proportionally to nodes' strengths.

[13] Epstein, J.M., Parker, J., Cummings, D., Hammond R.A. (2008) Coupled Contagion Dynamics of Fear and Disease Mathematical and Computational Explorations. *PLoS ONE* 3(12):e3955.

[14] Funk, S., Gilad, E., Watkins, C., Jansen, V.A.A. (2009) The spread of awareness and its impact on epidemic outbreaks. *Proc. Nat. Acad. Sci. USA* 106:6872-6877.

[15] Mexican Authorities, *Boletín Mensual de Estadística Operacional. Secretaría*

de comunicaciones y transportes (2009).

[16] Colizza, V., Barrat, A., Barthelemy, M., Vespignani, A. (2006). The role of the airline transportation network in the prediction and predictability of global epidemics. *Proc. Nat. Acad. Sci. USA* 103: 2015-2020.

[17] Colizza, V., Barrat, A., Barthelemy, M., Valleron, A.J., Vespignani, A. (2007) Modeling the Worldwide Spread of Pandemic Influenza: Baseline Case and Containment Interventions. *PLoS Med*, 4(1):e13.

[18] Germann, C., Kadau, K., Longini, I.M., Macken, C.A. (2006). Mitigation strategies for pandemic influenza in the United States. *Proc. Nat. Acad. Sci. USA* 103:5935-5940.

[19] Epstein, J.M. et al (2007) Controlling Pandemic Flu: The Value of International Air Travel Restrictions. *PLoS ONE* 2(5):e401.